Received: 22 October 2018 | Revised: 18 March 2019 | Accepted: 19 March 2019 | Published on: 08 May 2019

DOI: 10.1002/qj.3529

RESEARCH ARTICLE

Quarterly Journal of the Royal Meteorological Society RMetS

Tropical cyclogenesis at and near the Equator

Sian C. Steenkamp | Gerard Kilroy | Roger K. Smith

Meteorological Institute, Ludwig Maximilian University of Munich, Munich, Germany

Correspondence
Gerard Kilroy, Meteorological Institute, Ludwig Maximilian University of Munich, Theresienstrasse 37, 80333 Munich, Germany.
Email: gerard.kilroy@lmu.de

Abstract

The formation of tropical cyclones within a few degrees latitude of the Equator is investigated using European Centre for Medium-Range Weather Forecasts (ECMWF) analyses of some prominent cyclogenesis events there. The possibility of formation at the Equator is demonstrated also using idealized model simulations, starting from a prescribed, weak (maximum wind speed 5 m/s) initial counter-clockwise vortex in an otherwise quiescent, non-rotating environment.

In the real events investigated, vortex formation occurred within a broadscale counter-clockwise flow that encompasses a region of predominantly positive absolute vertical vorticity typically extending more than 5° south of the Equator. Patches of enhanced vertical vorticity form within this region as a result of vorticity stretching by deep convection. These vorticity patches are organized by the convection, the collective effects of which produce an overturning circulation that fluxes vorticity at low levels towards some centre within the convective region. By Stokes' theorem, the tangential circulation about circles of fixed radius around this centre increase and the vortex spins up. This process of spin-up is the same as that which occurs away from the Equator.

KEYWORDS

tropical cyclogenesis, tropical depressions, tropical lows

1 | INTRODUCTION

It used to be thought that tropical cyclones do not form within about 5° of the Equator on the grounds that at such low latitudes the Earth's background rotation is insufficient to support vortex spin-up (e.g., Anthes, 1982, p. 48; Gill, 1982, p. 476; Houze, 1993, p. 406; Pielke and Pielke, 1997, p. 82; Wallace and Hobbs, 2006, p. 369). As noted by Emanuel (2005, p. 97), this thought was proved to be incorrect by the occurrence of Typhoon *Vamei*, which was first classified as a tropical depression at a latitude of about 1.5°N on December 26, 2001 over the South China Sea and made landfall one day later along the southeastern coastline of the Malay Peninsula at 1.6°N, about 50 km north of Singapore. As it turns out, Typhoon *Vamei* was not an isolated event. In fact, in the International Best Track Archive for Climate Stewardship (IBTrACS; see Knapp *et al.*, 2010 for more information) there are 34 tropical cyclones listed that formed between 3°N and 3°S, 87 that formed between 4°N and 4°S and 213 that formed between 5°N and 5°S during the period 1900–2017. The majority of these low-latitude tropical cyclones formed in the Northern Hemisphere Western Pacific.

The intensification of low-latitude storms has been found also in numerical simulations, but mostly in passing, and it appears not to have been investigated in detail. In an idealized numerical study of tropical cyclogenesis by Montgomery *et al.* (2006), a simulation was carried out in which the planetary vorticity was set to zero. In this simulation, the initial vortex, which had a maximum wind speed of 6.6 m/s was located at a height of 4 km, underwent a period of spin-up to produce a short-lived depression that decayed within a few days. A similar simulation is presented here in section 2.

In a presentation at the 33rd American Meteorological Society Conference on Hurricanes and Tropical Meteorology, Hobgood (2018) proposed that the term in the expression for the Coriolis that involves the vertical velocity w and the cosine of latitude may be important in providing an explanation for the source of rotation of storms that form near the Equator. This term is normally neglected on the basis of scaling arguments. At least in global hydrostatic models, its inclusion in the approximate equations of motion on a spherical Earth leads to a spurious energy source and a lack of an angular momentum principle (Phillips, 1966).

Hobgood noted that typical values for w assumed in scaling midlatitude flows are on the order of 10^{-2} m/s, while values in the updraughts of tropical deep convection are two orders of magnitude larger than this. Moreover, since the cosine of latitude is a maximum at the Equator, he argued that the term involving w would be no more than an order of magnitude less than the Coriolis force calculated for midlatitudes. However, the idealized numerical simulations referred to above include the contribution to the Coriolis term involving w, and these terms are not present in the European Centre for Medium-Range Weather Forecasts (ECMWF) forecast model upon which the Centre's analyses are, in part, based (N. Wedi, personal communication). These facts would seem to suggest that the w contribution to the Coriolis force is not necessary for explaining vortex spin-up near the Equator.

The present study seeks an improved understanding of the intensification of lows near the Equator. To this end, we examine briefly in section 2 three idealized numerical simulations of tropical cyclogenesis that are similar to the zero-latitude case reported by Montgomery *et al.* (2006). Then we proceed to examine the evolution of four low-latitude events including Typhoon *Vamei* (2001), Super Typhoon *Dolphin* (2015), Tropical Depression 9C (2015–2016) and Hurricane *Pali* (2016), a storm that developed over the central North Pacific. The study of these events is based on data provided by ECMWF analyses.

The analysis methodology and the ECMWF datasets are described in section 3, while the events themselves are examined in sections 4–6. Conclusions are presented in section 7.

2 | IDEALIZED NUMERICAL SIMULATIONS WITH ZERO CORIOLIS PARAMETER

As a first step in investigating the spin-up of tropical cyclones near the Equator, we perform three idealized numerical experiments using the state-of-the-art CM1 model (version 16) with high horizontal resolution (grid spacing 500 m). CM1 is a non-hydrostatic and fully compressible cloud model (Bryan and Fritsch, 2002). The experimental set-up is essentially the same as that described in Kilroy and Smith (2017), who used it to investigate the effects of initial vortex size on hurricane genesis and intensification. Experiment 1 (E1) is initialized with a small initial vortex in which the radius of maximum winds, R_{vmax}, equals 50 km. In Experiment 2 (E2), R_{vmax} equals 100 km, while in Experiment 3 (E3) it equals 150 km. The maximum tangential wind speed of the initial vortices (5 m/s) occurs at the surface. The larger the initial radius, the broader is the core of cyclonic vorticity and the larger the source of cyclonic angular momentum available for spin-up. The choice of a surface-based initial vortex instead of an initial mid-level vortex is supported by the case studies presented in sections 4–6 and by the analysis of lows that developed within the Australian monsoon (Smith *et al.*, 2015; Kilroy *et al.*, 2016, 2017b). In the majority of these case studies, vortex development occurred first at low levels with no evidence of an accompanying mid-level vortex. The initial vortices are warm-cored, axisymmetric and cloud-free, although the warm core is extremely weak, the maximum temperature difference from the ambient temperature being only 0.1 K and located on the axis at a height of 15 km. The only difference in the configuration of the experiments described here is that the Coriolis parameter f is set equal to zero, corresponding to the Equator, whereas in Kilroy and Smith (2017) $f = 2.53 \times 10^{-5}$ s^{-1}, corresponding to 10°N.

The domain is $3,000 \times 3,000$ km in size with an inner domain of 300×300 km in which there is a uniform horizontal grid spacing of 500 m. Elsewhere the grid spacing is stretched to the outer boundary. The domain has 40 vertical levels beginning at a height of 25 m and extending to a height of 25 km. The vertical grid spacing is stretched with increasing height. For simplicity we employ warm-rain microphysics only (the Kessler scheme) and radiative effects are represented by a simple Newtonian cooling capped at 2 K per day. More details about the model set-up are given in sect. 2 of Kilroy and Smith (2017). The main aim of the present section is to determine in broad terms how the genesis and subsequent intensification are affected by having no ambient rotation, that is, $f = 0$ s^{-1}.

2.1 | Vortex evolution

Figure 1 shows a time series of the azimuthally averaged maximum tangential wind speed (V_{max}) for E1 (red line), E2 (blue line) and E3 (yellow line) out to 108 hr. The evolution is similar to that found in Kilroy and Smith (2017, their fig. 2a). Namely, the V_{max} curves for all three simulations are essentially identical until about 36 hr. At this time the vortex in E1 undergoes a period of rapid intensification (RI). The vortex in E2 begins its RI phase about 12 hr later, while in E3 the RI phase is delayed by a further 10 hr. Significantly, the intensification begin times in all three experiments are almost identical to those in the corresponding experiments for 10°N described by Kilroy and Smith (2017), suggesting that the ambient rotation is not an important factor in the

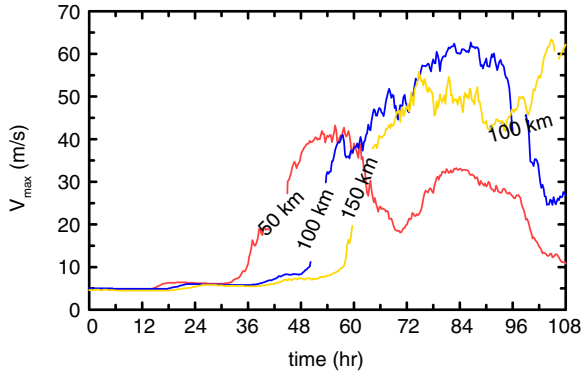

FIGURE 1 Time series of maximum azimuthally averaged tangential wind speed (V_{max}) in the idealized numerical simulations with zero Coriolis parameter: Experiment 1 (labelled 50 km), Experiment 2 (labelled 100 km) and Experiment 3 (labelled 150 km) [Colour figure can be viewed at wileyonlinelibrary.com]

genesis of tropical cyclones, at least within 10 degrees of the Equator.

A notable difference in the evolution of the vortices shown here is that their life cycle is relatively short, with those in E1 and E2 showing appreciable decay within the 4.5 days of simulation time, and that in E3 showing signs of decay near the end of this period. In comparison, at 10°N, all three vortices are still intensifying at 4.5 days. Here, the vortex in E1 has all but decayed at this time, with V_{max} being only about 10 m/s. Another notable difference is the lifetime maximum of V_{max}, which is much smaller when $f = 0\,s^{-1}$. For example, the lifetime maximum V_{max} in E1 is approximately 43 m/s, compared with 67.5 m/s at 10°N. In E2 and E3, the lifetime maxima of V_{max} are approximately 63 and 64 m/s, respectively, compared with 80 and 88 m/s when the vortices are located at 10°N. The reason for the early decay of vortices at the Equator is the limited source of cyclonic vorticity or angular momentum, which both decrease with decreasing initial vortex size.

In summary, genesis and subsequent rapid intensification occur in idealized numerical simulations when the Coriolis parameter is set to zero. Interestingly, without Coriolis forces, the intensification begin time is the same as for vortices located at a latitude of 10°N. The vortices developing on the Equator ($f = 0\,s^{-1}$) are weaker than those developing at 10°N and begin to decay much sooner. These findings suggest that the Coriolis force is not important in the genesis of tropical cyclones, although it is important for maintaining intensification in longer-lived storms. Further analysis of the foregoing simulations will be presented in a future study.

3 | ECMWF ANALYSES AND METHODOLOGY

Recent theoretical work has led to the development of a new paradigm for both tropical cyclogenesis and tropical cyclone intensification, the so-called rotating convection paradigm. Reviews of this paradigm and its relationship to previous theories of tropical cyclone behaviour are provided by Montgomery and Smith (2014, 2017), Smith and Montgomery (2016), and Smith *et al.* (2017). In essence, the new paradigm constitutes an overarching framework for interpreting the complex vortex-convective phenomenology in simulated and observed tropical cyclones. The paradigm explicitly recognizes the presence of localized, rotating deep convection whose vorticity is amplified greatly over that of the broad-scale vortex circulation by vortex-tube stretching and tilting processes. The paradigm includes an azimuthally averaged description of storm behaviour that takes into account the effect of locally asymmetric (or eddy) processes.

From a vorticity perspective, an important mechanism for the intensification of an existing vortical circulation is the inward flux of absolute vorticity into the vortex in the lower troposphere brought about by inflow produced there by the collective effects of deep convection. This is, in essence, the classical mechanism for intensification articulated by Ooyama (1969) and is reviewed in detail in sect. 4 of Montgomery and Smith (2017). Following Smith *et al.* (2015) and Kilroy *et al.* (2016, 2017b), we examine the genesis of several storms from a vorticity perspective using data provided by ECMWF analyses. In particular, we focus here on the reservoir of absolute vorticity required to support vortex intensification.

3.1 | Data

The data for the subsequent analyses are taken from the ECMWF analyses, which are available at 6 hr intervals from 0000 universal time coordinated (UTC) and with a horizontal grid spacing of 0.125°. For Typhoon *Vamei* the data are available at 21 pressure levels starting from 1,000 mb and decreasing to 1 mb, while for the later storms (Super Typhoon *Dolphin*, Tropical Depression 9C and Hurricane *Pali*) they are available at 25 levels in the same pressure range.

4 | TYPHOON *VAMEI* (DECEMBER 2001)

A few details of Typhoon *Vamei* were discussed in the Introduction. The best track for this typhoon as determined by the Joint Typhoon Warning Center (JTWC) is shown in Figure 2, together with that determined by the location of the minimum geopotential height at 1,000 mb in the ECMWF analyses. In both cases, the locations are shown at 6 hr intervals. The two tracks overlap well between December 26 and December 28, especially when *Vamei* is over the southern Malay Peninsula on December 27.

4.1 | Synoptic setting and intensity

The precursor low appears to have been the so-called Borneo vortex, which is a feature of the seasonal climatology in the

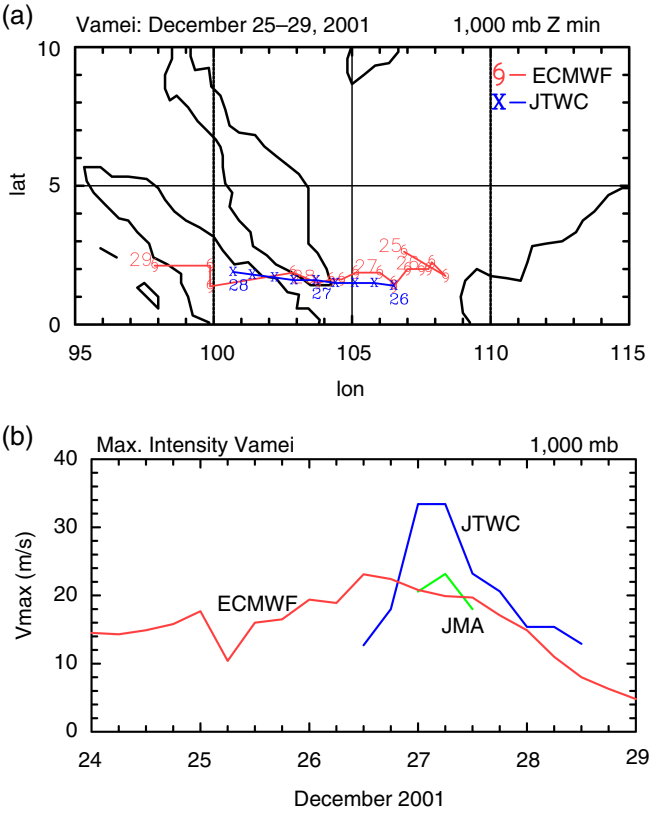

FIGURE 2 (a) The Joint Typhoon Warning Center (JTWC) best track for Typhoon *Vamei* (blue curve) and the track determined from the ECMWF analyses (red curve) by locating the minimum geopotential height at 1,000 mb. The JTWC best track starts at 1200 UTC on December 26 and is given at 6 hr intervals. The maximum winds for Typhoon *Vamei* are shown in panel (b). The maximum wind speeds from the JTWC are available for the period between 1200 UTC on December 26 and 1200 UTC on December 28 (blue curve). The data from the Japanese Meteorological Agency (JMA) are available for only three times: 0000 UTC, 0600 UTC and 1200 UTC on December 27 (green curve). The ECMWF wind speeds are denoted by the red curve [Colour figure can be viewed at wileyonlinelibrary.com]

region (Chang and Wong, 2008). In essence, the Borneo vortex is a cyclonic circulation located over the South China Sea to the northwest of Borneo that is associated with periodic cold surges. These surges are accompanied by northeasterly winds that herald an intensification of the Asian winter monsoon associated with a strengthening of the Siberian High (Koseki *et al.*, 2014).

At 0000 UTC on December 25, the precursor low in the ECMWF analyses was located to the west of Borneo at around 3°N, 107°E (Figure 2a) and over the next 24 hr tracked slowly southeastwards. It was classified by the Japanese Meteorological Agency (JMA) as a tropical depression (TD) at 1200 UTC on December 26. The JTWC upgraded the low to Tropical Storm (TS) *Vamei* at 1800 UTC on December 26, when its centre was located at about 1.5°N, 105.8°E, and further upgraded it to Typhoon *Vamei* at 0000 UTC on December 27 based on maximum wind speeds of between 33 and 39 m/s measured by naval ships (Juneng *et al.*, 2007; Chang and Wong, 2008). At this time the typhoon was moving westwards towards the Malay Peninsula.

The estimated maximum wind speeds obtained from the JTWC and JMA best track data and those from the ECMWF analyses are shown in Figure 2b. The maximum winds from the ECMWF analyses are calculated at 1,000 mb within a $2° \times 2°$ region centred around the low. The intensity determined by the JMA and that derived from the ECMWF analyses are similar from 0000 UTC to 1200 UTC on December 27, with maximum wind speeds around 20 m/s. However, as noted above, the JTWC estimated the maximum wind speeds to be considerably higher.

Typhoon *Vamei* made landfall about 50 km northeast of Singapore at 0830 UTC on December 27 (Chang and Wong, 2008). Even though the storm weakened somewhat after it had made landfall, it still produced heavy rainfall in the region, with a station in Senai measuring in excess of 200 mm (Juneng *et al.*, 2007). The storm continued to weaken as it tracked westwards over the Malacca Strait and over the northern parts of Sumatra until it was downgraded to TD status at 0000 UTC on December 28. By December 29, the remnants of *Vamei* were located northwest of Sumatra.

The evolution of *Vamei* is exemplified by selected fields from the ECMWF analyses shown in Figure 3. These fields include the absolute vorticity distribution, the geopotential height field and the horizontal wind vectors at 850 mb, together with the vertical p-velocity, ω (the material derivative of pressure, p), at 500 mb.

4.2 | Absolute vorticity

As indicated in section 3, we examine the evolution of *Vamei* principally from a vorticity perspective based on the ECMWF analyses. To this end, the first four panels of Figure 3 show the absolute vorticity distribution. Within 5° of the Equator, values of f are relatively small, less than 1.3×10^{-5} s^{-1}, so that the absolute vorticity, ζ_a, is dominated by relative vorticity, ζ. In some localized regions, ζ can exceed 5×10^{-4} s^{-1} in magnitude, long before any named TD has formed (not shown). However, as the latitude increases, the contribution of f to ζ_a becomes progressively more important.

An increase in the strength of the northeasterly winds from 0000 UTC on December 23, 2001 is accompanied by the development of a low-level cyclonic (counter-clockwise) circulation northwest of Borneo (not shown). This cyclonic circulation is indicative of the development of the Borneo vortex and is seen at 1800 UTC on December 24 in Figure 3a at around 108°E, 3°N. The low develops just north of the Equator in an extensive region of positive absolute vorticity that extends well into the Southern Hemisphere at this time. A prominent feature of the absolute vorticity field is a comma-shaped region of enhanced positive ζ_a ($> 1 \times 10^{-4}$

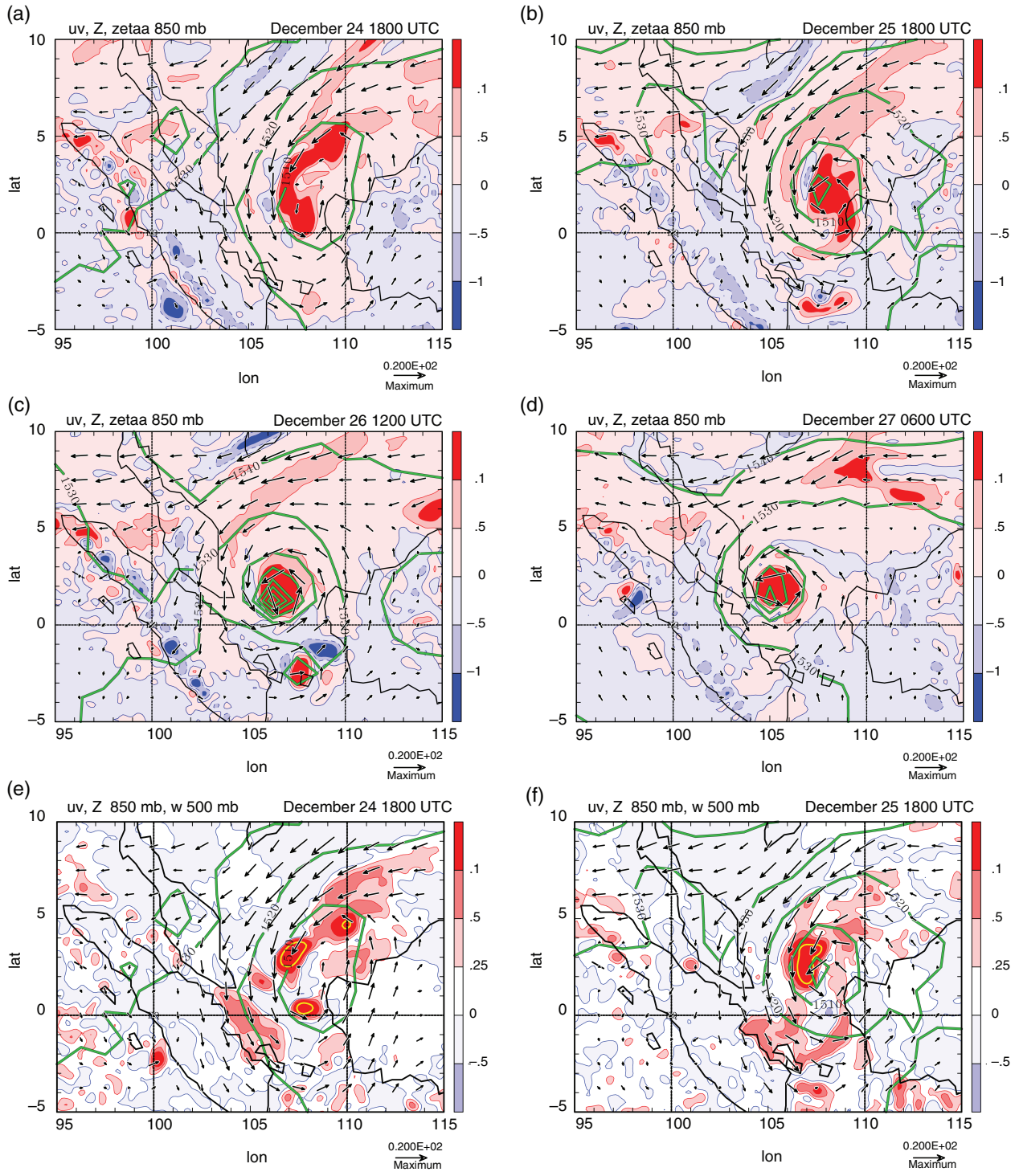

FIGURE 3 Horizontal cross-sections of wind vectors and geopotential height at 850 mb together with (a–d) absolute vorticity at 850 mb, ζ_a, and (e,f) vertical p-velocity at 500 mb, ω, during the genesis and evolution of Typhoon *Vamei* at the times shown. The scale for wind vectors is given in m/s at the bottom right. Geopotential height is in geopotential metres (gpm) (solid green contours, interval 10 gpm). In panels (a–d), the red shading indicates counter-clockwise vorticity (cyclonic in the Northern Hemisphere, anticyclonic in the Southern Hemisphere) and blue shading indicates clockwise vorticity (shading values are multiplied by 1×10^{-4} s^{-1}). In panels (e) and (f), positive vertical velocity (negative ω) is shaded red, while negative vertical velocity (positive ω) is shaded light blue (units Pa/s). Red contours: 0.25, 0.5 and 1 Pa/s, respectively. Thick yellow contour: 2 Pa/s

s^{-1}), starting near the Equator and curving round to the north-east. This region is one also of low geopotential height. At the Equator itself, positive values of ζ_a extend from approximately 104°E to 110°E and the winds are northerly to the west of about 108°E and southerly to the east of this longitude, at least as far as 113°E. Clearly, there is a flux of positive absolute vorticity into the Southern Hemisphere between 104°E and 108°E and back from the Southern Hemisphere into the Northern Hemisphere between 108°E and 110°E. At longitudes west of 104°E, there is a flux of negative absolute vorticity from the Northern Hemisphere to the Southern Hemisphere and a similar return flux east of about 110°E.

During the 24 hr period leading up to 1800 UTC on December 25 (Figure 3b), the comma-shaped region of positive ζ_a has consolidated into a monopole of enhanced vorticity centred at about 108°E, 2°N with a comma-shaped tail, and the geopotential heights have fallen in the region of the monopole. Positive absolute vorticity continues to extend several degrees into the Southern Hemisphere.

By 1200 UTC on December 26 (Figure 3c), the vorticity monopole has continued to consolidate. The geopotential field now has a sharp minimum within, but slightly to the southwest of the monopole centre. The winds have increased in strength and the counter-clockwise circulation has become focussed around the vorticity monopole, extending well into the Southern Hemisphere. However, the extensive region of positive absolute vorticity that was south of the Equator has now retreated to the Northern Hemisphere.

Just before landfall over the Malay Peninsula at 0600 UTC on December 27 (Figure 3d), the vortex remains strong and compact, while the pool of absolute vorticity feeding around and into the low continues to be located mainly in the Northern Hemisphere. A counter-clockwise circulation still extends a few degrees into the Southern Hemisphere.

4.3 | Vertical velocity

The local amplification of vertical vorticity can be attributed in part to the vertical stretching of absolute vorticity, principally by deep convection (Hendricks *et al.*, 2004; Montgomery *et al.*, 2006; Nguyen *et al.*, 2008; Wissmeier and Smith, 2011; Kilroy and Smith, 2016; and references therein). It is therefore of interest to examine the vertical velocity distribution at 500 mb in the vicinity of *Vamei* and its precursor low. Regions of strong vertical velocity at this level indicate the presence of areas of deep convection (herein, by deep convection we refer to regions in the 500 mb analyses with $\omega \geq 1$ Pa/s, and by vigorous deep convection we refer to regions with $\omega \geq 2$ Pa/s) in the ECMWF analysis and forecasting system[1] and therefore regions with pronounced lower-tropospheric convergence and upper-tropospheric divergence.

Figure 3e,f shows the 500 mb vertical velocity at the same times as the vorticity in Figure 3a,b during the early evolution of *Vamei*. Comparison of Figure 3a and Figure 3e confirms, as expected, that regions of strong ascent tend to be co-located with regions of high vorticity (values $\geq 10^{-4}$ s^{-1}).

4.4 | Bulk properties

Figure 4 shows time–height cross-sections of selected spatially averaged quantities centred on Typhoon *Vamei* and its precursor low from December 24–29, 2001. These quantities include the vertical mass flux, the relative humidity (RH), the temperature deviation (dT) from the initial time and the pseudo-equivalent potential temperature (θ_e). These quantities are averaged at each pressure level over a $2° \times 2°$ square[2] column centred at the location of the minimum geopotential height at 850 mb. Shown also are the vertical shear, which is calculated by taking the vector difference of the horizontal winds between 850 and 200 mb and averaging over three square domains of $2° \times 2°$, $4° \times 4°$ and $6° \times 6°$, and the normalized circulation, which is defined as the line integral of the horizontal winds around the boundary of a $2° \times 2°$ box at a given pressure level, normalized by the geometric length of the boundary, taking into account the variation of longitudinal distance with latitude.

The ECMWF analyses has the maximum intensity of the system at 1200 UTC on December 26 (Figure 2a). This is 12 hr earlier than estimates from observations, which needs to be taken into consideration when interpreting the analyses. Irrespective of the averaging area used, the vertical shear remains modest during the entire development period, less than about 7 m/s, but increases to about 10 m/s in the smaller column at the time of peak near-surface wind speed in the analyses (Figure 4a). The vertical mass flux profile (Figure 4b) shows two "bursts" of enhanced mass flux prior to the maximum intensity and another burst at the time of peak intensity. The peak circulation is attained after this third burst at about 1800 UTC on December 26 and occurs at low levels, about 850 mb (Figure 4c). The relative humidity is generally high below the 500 mb level with little structural variation (Figure 4d). There is some warming on the order of 1 K accompanying the intensification, with slight cooling

[1]The ECMWF analysis and forecasting system is such that observational data are continuously assimilated using a four-dimensional variational scheme. The forecast model component from which vertical velocities are inferred does not have sufficient horizontal resolution to resolve individual deep convective systems explicitly, but uses a parameterization scheme to represent the effects of these systems. Therefore, one does not expect a faithful rendition of the details of observed convection. Even so, areas of deep convective activity appear to be captured reasonably well by the system (see, e.g., Smith *et al.*, 2015, p. 326).

[2]Note that the square is only approximate geometrically as it is defined in terms of latitude and longitude.

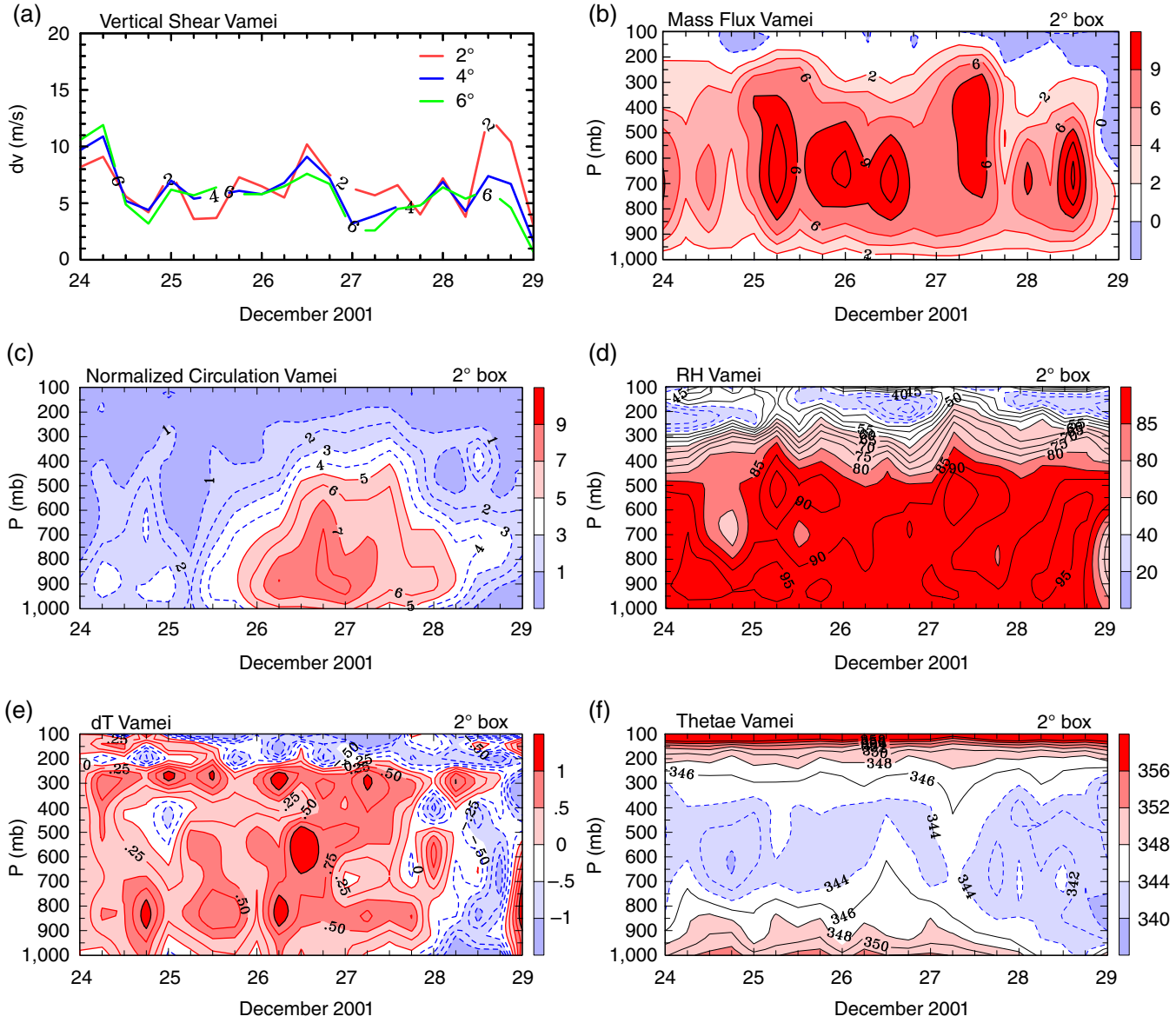

FIGURE 4 (a) Time series of vertical wind shear between 850 and 200 mb averaged over columns 2° × 2°, 4° × 4° and 6° × 6° centred at the location of the minimum geopotential height at 850 mb. Time–height cross-sections of various quantities are averaged over a 2° × 2° column centred on the low. Panel (b) shows the vertical mass flux (unit 10^{-2} kg s^{-1} m^{-2}). Contour intervals: solid red contours from 2×10^{-2} kg s^{-1} m^{-2} to 6×10^{-2} kg s^{-1} m^{-2} in intervals of 2×10^{-2} kg s^{-1} m^{-2}; black contours every 3×10^{-2} kg s^{-1} m^{-2} from 9×10^{-2} kg s^{-1} m^{-2}. The dashed blue contour is the zero contour. (d) Relative humidity (in %), with contours every 5% and dashed contours for values below 40%. (e) Temperature deviation from the start of the series (dT, unit K). Contour intervals: solid red contours from 0 to 0.75 K in intervals of 0.25 K; solid black contours in intervals of 0.5 K from 1.0 K. Dashed negative contours are every 0.25 K below −0.25 K. (f) Pseudo-equivalent potential temperature (θ_e, unit K). Contour intervals are every 2 K, with dashed blue contours below 344 K and solid black contours above 346 K. Panel (c) shows the circulation around the 2° × 2° column (unit m/s) normalized by the length of the boundary. Contours are every 1 m/s, with dashed blue contours for values below 4 m/s and solid red contours for values above 5 m/s. Shadings are as given by the sidebars [Colour figure can be viewed at wileyonlinelibrary.com]

occurring during the decay phase as the system tracks over land (Figure 4e). Further, there is an elevation of θ_e values in the mid-troposphere near peak intensity (Figure 4f). In terms of these spatially averaged quantities, the evolution of *Vamei*, which according to Chang *et al.* (2003) was a once every 100–400 years event, is largely consistent with that of tropical cyclones that develop off the Equator in the Australian monsoon (Smith *et al.*, 2015; Kilroy *et al.*, 2016, 2017b).

5 | SUPER TYPHOON *DOLPHIN* (MAY 2015)

The first advisory for the low that ultimately became Super Typhoon *Dolphin* was issued by the JTWC at 0000 UTC on May 5, 2015. At that time the low centre was located approximately 1,700 km northeast of Papua New Guinea, in a region where sea surface temperatures were over 1°C higher than

normal as a result of relatively strong El Niño conditions. The JTWC classified the low as a TD at 1800 UTC on May 6 when its position was estimated to be approximately 4.5°N, 158.9°E. The track from the ECMWF analyses and the best track from the JTWC are shown in Figure 5a for the period May 6–15. These tracks largely overlap, an indication that the location of the low is well captured by the ECMWF analyses. For the first two days the low moved approximately east-southeastwards, reaching a minimum latitude of 3°N before recurving progressively to the north and later to the northwest.

Figure 5b compares the time series of the maximum wind speed at 1,000 mb determined from the ECMWF analyses with that from the JTWC best track data. The low was named by the JTWC as TS *Dolphin* at 1200 UTC on May 8 with estimated maximum near-surface winds of 18 m/s (35 knots). It was later upgraded to Typhoon *Dolphin* when located at 10°N, 156°E and finally to Super Typhoon status on May 16 when it had 1-min sustained winds of 72 m/s (140 knots). The ECMWF analyses estimate the maximum wind speed remarkably well up to about 0000 UTC on May 13, but underestimate it beyond this time as the low increases in intensity.

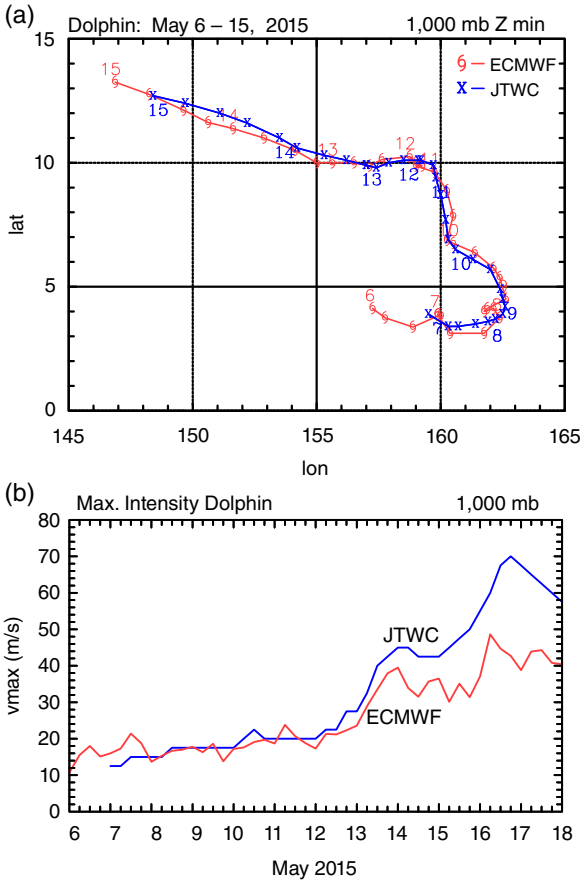

FIGURE 5 (a) Track of the low that developed over the Northwest Pacific in May 2015 and became Super Typhoon *Dolphin*. The ECMWF track (red curve) is shown together with the best track data of the JTWC (blue curve). Panel (b) shows the ECMWF (red curve) maximum horizontal velocity at 1,000 mb and the maximum winds according to the JTWC best track data (blue curve) [Colour figure can be viewed at wileyonlinelibrary.com]

5.1 | Vortical and convective environment

Of primary interest in this section is the early development of the low that ultimately became Super Typhoon *Dolphin*. To determine the origin of this low, it proved necessary to step back in time to 0000 UTC on May 1, 5 days before the first advisory was issued. Figure 6 shows the absolute vorticity, horizontal winds and geopotential height, all at 850 mb, together with the vertical *p*-velocity at 500 mb during these formative stages.

At 0000 UTC on May 1 there is a clearly defined horizontal shear zone north of the Equator with westerly winds extending from 130°E to about 160°E and to at least 3°N and with easterlies poleward of about 9°N (Figure 6a). The shear zone is marked by three prominent patches of enhanced absolute vorticity, one near the western boundary of the domain shown, one centred near 150°E, 7°N, which is marked also by a weak cyclonic circulation and a region of low geopotential height, and one centred in the vicinity of 164°E, 7°N. This easternmost patch, which shows also a slight lowering of the geopotential height, marks the precursor low to Super Typhoon *Dolphin*. Deep convection, as characterized by regions of strong ascent at 500 mb, is patchy across the shear zone, but regions of deep convection are located in proximity to the regions of enhanced absolute vorticity (Figure 6b).

Two days later, at 0000 UTC on May 3, the westernmost patch of enhanced absolute vorticity has moved out of the domain shown. The central patch has become more organized and has developed a significant cyclonic circulation. The geopotential heights have deepened further also (Figure 6c). There is an area of deep convection located near the circulation centre (Figure 6d), which is particularly favourable for further development (Smith and Montgomery, 2016, sect. 4). At this time, the low is located near 142°E, 8°N. Eighteen hours later, the JMA named this low TS *Noul* and the storm later developed into Super Typhoon *Noul*. The easternmost patch of enhanced absolute vorticity (now located at roughly 155°E, 6°N) remains somewhat elongated, but the wind field shows an increased cyclonic circulation from 2 days earlier. This patch of absolute vorticity is co-located with a patch of deep convection.

At 0000 UTC on May 5, the precursor low to Super Typhoon *Dolphin* is now located near 157°E, 4°N, but the absolute vorticity has become somewhat sheared in the horizontal by the increasing easterly winds to the north and westerlies to the south, the latter associated with a "westerly wind burst" (Figure 6e). Nevertheless, the region of enhanced absolute vorticity remains located in an extensive area of sustained deep convection. As a result, while still showing some effects of horizontal shear, the vorticity becomes more organized during the following day.

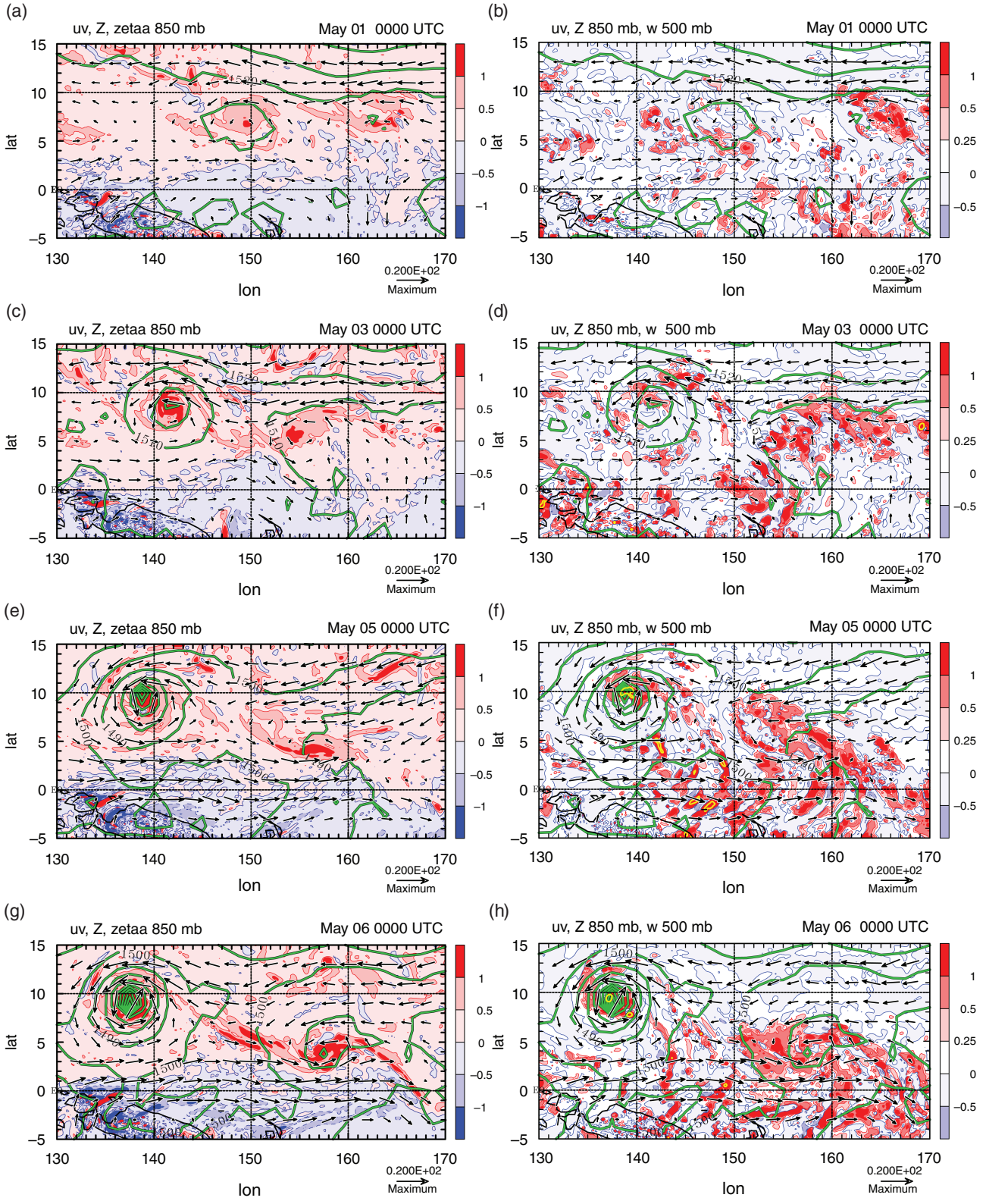

FIGURE 6 Horizontal cross-sections of wind vectors and geopotential height at 850 mb together with absolute vorticity at 850 mb, ζ_a (left panels), and vertical p-velocity at 500 mb, ω (right panels), during the genesis and early evolution of Super Typhoon *Dolphin* at the four times shown. The scale for wind vectors is given in m/s at the bottom right. Geopotential height is in geopotential metres (gpm) (solid green contours, interval 10 gpm). In the left panels, the red shading indicates counter-clockwise vorticity (cyclonic in the Northern Hemisphere, anticyclonic in the Southern Hemisphere) and blue shading indicates clockwise vorticity (shading values are multiplied by 1×10^{-4} s^{-1}). In the right panels, positive vertical velocity (negative ω) is shaded red, while negative velocity (positive ω) is shaded light blue (units Pa/s). Red contours: 0.25, 0.5 and 1 Pa/s, respectively. Thick yellow contour: 2 Pa/s

By 0000 UTC on May 6 the low of interest is indicated by two closed isopleths of geopotential height and absolute vorticity. It has become more organized with a bulge near this centre, but remains somewhat elongated, presumably on account of the continued action of the strong broadscale horizontal shear (Figure 6g). Deep convection continues to be active across the low, indicating the potential for further development (Figure 6h). At 1800 UTC on May 6, the JTWC classified the system as a TD.

As indicated in Figure 5, this depression tracked east-southeastwards during May 6 and 7, presumably because of the dominant influence of the strong westerly flow to the south. Thereafter, the low recurved to the north and later to the northwest.

The genesis of the aforementioned pair of super typhoons fits the classical model for the breakdown in the Intertropical Convergence Zone (ITCZ) as described in a nonlinear shallow water model on the sphere by Ferreira and Schubert (1997, p. 261). This model idealizes the ITCZ as a zonally elongated mass sink near the Equator. The mass sink generates a cyclonic potential vorticity (PV) anomaly that has a reversed meridional PV gradient on its poleward side. This reversed gradient may lead to an instability of the flow in the presence of small disturbances. Ferreira and Schubert show that the unstable PV strip either undulates and breaks down into several cyclones or axisymmetrizes into one large cyclone. They suggest that this kind of "ITCZ breakdown may play a role in producing the observed tendencies for tropical storms to cluster in time and form poleward of the central latitude of the ITCZ and to the east of existing tropical storms," which is precisely the situation described above.

6 | TD-9C (DECEMBER 2015) AND HURRICANE *PALI* (JANUARY 2016)

In late December 2015 and early January 2016, the equatorial region of the Central Pacific became convectively active resulting in the formation of two tropical lows, the second of which became Hurricane *Pali*. At 1500 UTC on January 7, 2016, the Central Pacific Hurricane Center (CPHC) in Honolulu referred to the low as TD-1C, but later renamed it TS *Pali*. TS *Pali* intensified progressively and was classified as a Category 1 hurricane at 0300 UTC on January 12, 2016 when its circulation centre was located around 8.1°N, 171.9°W. At that stage, the storm had maximum sustained winds of 37 m/s (75 knots) and a central pressure of 982 mb.

Our interest herein is focussed on the genesis of Hurricane *Pali* as well as a TD designated TD-9C by the CPHC at 0300 UTC on December 31, 2015, which preceded Hurricane *Pali* by about a week. TD-9C formed to the west of the International Date Line and at an early stage the disturbance centre was just south of the Equator.

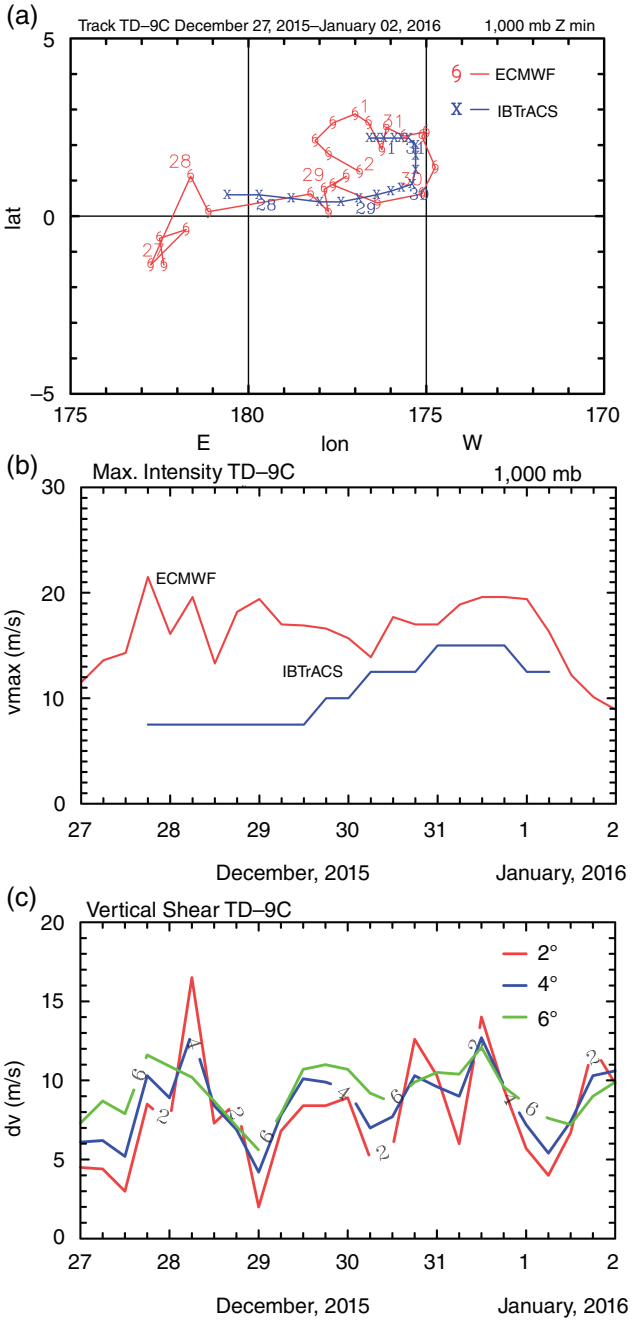

FIGURE 7 (a) Track of TD-9C from the ECMWF analyses (red curve) with the best track data according to IBTrACS (blue curve). Panel (b) shows the maximum intensity calculated from the ECMWF analysis data (red curve) with the best track data from IBTrACS (blue curve). Shown in panel (c) is the area-averaged vertical shear between 850 and 200 mb for areas 2° × 2° (red line), 4° × 4° (blue line) and 6° × 6° (green line) centred on the geopotential minimum at 850 mb [Colour figure can be viewed at wileyonlinelibrary.com]

6.1 | TD-9C

The track of TD-9C in the ECMWF analysis data is shown in Figure 7a. At 0000 UTC on December 27, the low centre was located in the Southern Hemisphere at around 1°S, 171.9°E, but after venturing to about 1.5°S it moved northeastwards

into the Northern Hemisphere and then eastwards to within a degree of the Equator until December 30, 2015. The low then turned to the north and later to the west, but by the end of January 1, 2016 it had decayed. In the CPHC report on TD-9C (Houston and Birchard, 2016), its development is noted to be "related to a belt of anomalously strong low-level westerly winds that was located along and just south of the equator toward the end of December 2015. The low-level convergence and upper level diffluence associated with these strong westerly winds allowed deep convection to develop and persist for a few days prior to the end of the calendar year, even though the last day of the official Central Pacific 2015 hurricane season was on 30 November."[3] The CPHC noted also the above-normal sea surface temperatures present in the Central Pacific as a result of the strong El Niño conditions during the genesis and intensification of TD-9C. It is worth pointing out that during the development of TD-9C, there was a relatively strong active phase of the Madden–Julian Oscillation (MJO) located over the Western Pacific. As it progressed eastwards, this MJO may have played a role in providing favourable environmental conditions to support deep convection near the centre of the developing system.

Figure 7b,c shows the maximum wind speed at 1,000 mb and the area-averaged vertical shear between 850 and 200 mb as in Figure 4a, but for TD-9C based on the ECMWF analyses. Figure 7b shows also the intensity estimate from IBTrACS, which was available for the period 1800 UTC, December 27 to 0600 UTC, January 1. The maximum wind speed of just over 21 m/s in the ECMWF analysis occurred at 1800 UTC on December 27. Thereafter this wind speed fluctuated between a minimum of about 14 m/s at 1200 UTC on December 28 and a maximum of about 19 m/s at 1200 UTC on December 31. For the period when they are available, the IBTrACS intensity estimates are several m/s lower than those from the ECMWF analyses, but their uniformity together with the uniform purely westward track from 1200 UTC on December 31 in Figure 7a makes one suspicious of their accuracy.

During the period shown, the vertical shear is generally below 10 m/s, but there are significant fluctuations over 6 hr time intervals. Moreover, there is little obvious correlation between changes in the shear and changes in intensity.

6.1.1 | Vortical and convective environment

Figure 8 shows the 850 mb absolute vorticity, horizontal winds and geopotential height at 850 mb together with the vertical p-velocity at 500 mb during the development of TD-9C. At 1200 UTC on December 25 (Figure 8a), the region between 165°E and the Date Line shows strips of elevated absolute vorticity (mostly relative vorticity) in the latitude band from 2°S to 2°N sandwiched between easterly trade winds to the north and monsoonal westerly winds to the south. Notably, the strips of elevated vorticity are located within an area of active deep convection (Figure 8b). At this time, geopotential height gradients are relatively weak, as is typical of the near-equatorial region. In particular, the two small areas of closed geopotential contours in regions of deep convection are transient features with no obvious connection to the subsequent evolution of TD-9C. Moreover, at this stage there is no obvious closed circulation within the region of horizontal shear.

At 0000 UTC on December 27, a closed circulation has formed about a small closed contour of low geopotential height which is situated just south of the Equator at about 178°E, 1°S (Figure 8c). The broadscale counter-clockwise circulation extends to at least 8° latitude from the centre in both hemispheres and there is a large incursion of positive (counter-clockwise) absolute vorticity into the Southern Hemisphere. Within this region of positive vorticity there are patches of enhanced values stretching from just south of the Equator, near the location of minimum geopotential height, and extending northeastwards in a curved band that extends to about 5°S before turning back towards the Equator. In this band there are numerous patches of vigorous deep convection with one patch located over the centre of the closed contour of minimum geopotential height (Figure 8d).

A day later, at 0000 UTC on December 28, the winds have strengthened around the low and the circulation centre is now slightly north of the Equator. The absolute vorticity has strengthened and consolidated near the centre of circulation, but the geopotential heights have fallen only slightly (Figure 8e). Deep convection remains vigorous within the broadscale circulation, although at this time the strongest convection occurs outside the closed contour of lowest geopotential height shown (Figure 8f). The low continues to reside in an environment of positive absolute vorticity that extends to 5°S over the 40° of longitude shown and as far south as 8°S near the longitude of the low centre. The considerable organization of the vorticity over the foregoing period of three days seen in Figure 8a,c,e takes place in the absence of an appreciable deepening of the vortex, consistent with the findings of Kilroy *et al.* (2017a) in an idealized study of tropical cyclogenesis.

Three days later at 0000 UTC on December 31, the system has drifted northwards while increasing in intensity (Figure 8g,h). At this time the absolute vorticity has formed into a coherent monopole within the broadscale circulation and there is a patch of vigorous deep convection just to the north of the circulation centre and slightly to the west of the minimum geopotential. This would seem to be a situation conducive to further intensification of the system, but just over a day later the system began to rapidly decay. Nevertheless,

[3]We do not endorse these causal interpretations on the grounds that deep convection itself *leads to* low-level convergence and upper-level divergence (not *diffluence*, which refers to horizontally non-divergent flow behaviour).

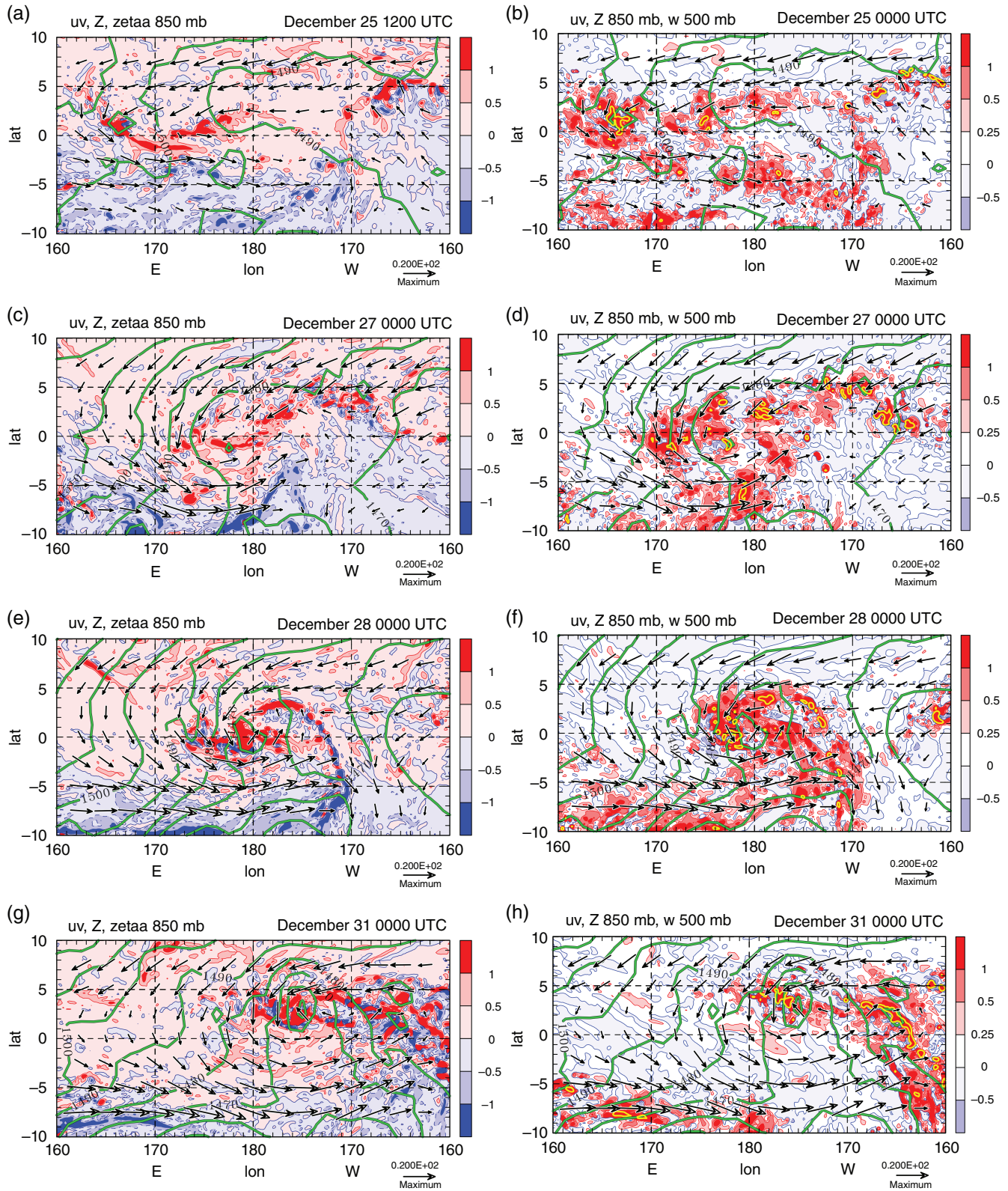

FIGURE 8 Horizontal cross-sections of wind vectors and geopotential height at 850 mb together with absolute vorticity at 850 mb, ζ_a (left panels), and vertical p-velocity at 500 mb, ω (right panels), during the genesis of TD-9C at the four times shown. The scale for wind vectors is given in m/s at the bottom right. Geopotential height is in geopotential metres (gpm) (solid green contours, interval 10 gpm). In the left panels, the red shading indicates counter-clockwise vorticity (cyclonic in the Northern Hemisphere, anticyclonic in the Southern Hemisphere) and blue shading indicates clockwise vorticity (shading values are multiplied by 1×10^{-4} s^{-1}). In the right panels, positive vertical velocity (negative ω) is shaded red, while negative velocity (positive ω) is shaded light blue (units Pa/s). Red contours: 0.25, 0.5 and 1 Pa/s, respectively. Thick yellow contour: 2 Pa/s

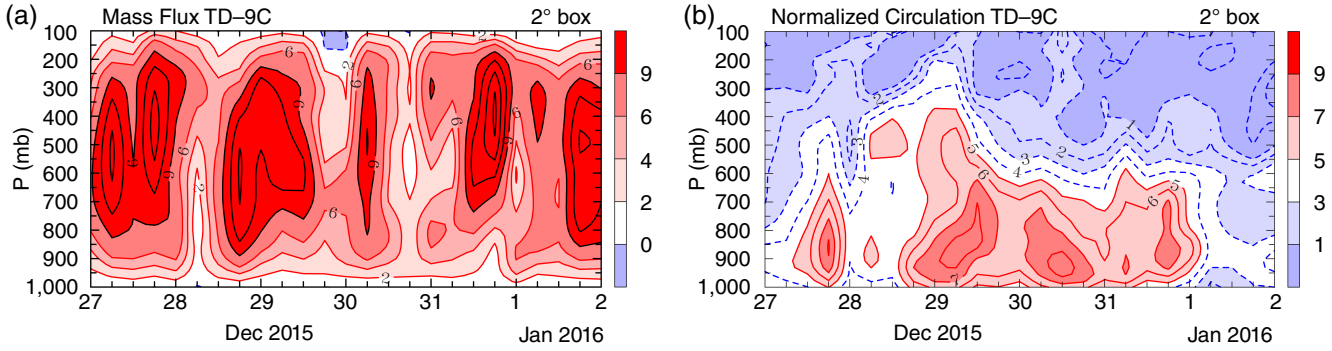

FIGURE 9 (a) Time–height cross-sections of vertical mass flux averaged over a 2° × 2° column centred at the minimum geopotential height at 850 mb for TD-9C. (b) Normalized circulation around the 2° × 2° column. The panels have the same descriptions as those in Figure 4 [Colour figure can be viewed at wileyonlinelibrary.com]

a broadscale shear zone remained in the region and it was within this shear zone that the precursor low of Hurricane *Pali* formed. The reasons for the decay of TD-9C are discussed in section 6.4.

6.1.2 | Bulk properties

Figure 9 shows a time–height cross-section of the vertical mass flux averaged over a 2° × 2° column centred on the minimum geopotential height together with the circulation around this column. The two bursts of "deep convection" on December 27 lead to a temporary spin-up of the circulation, and a more prolonged burst that starts at 1200 UTC on December 28 is accompanied by further spin-up. Surprisingly, convection persists within the column even though the circulation decreases in strength after 0000 UTC on January 1. This suggests that there are other factors inhibiting the system from developing (see section 6.4 below).

The circulation is strongest below heights corresponding to about 850 mb throughout the period of intensification; that is, this is a clear "bottom-up" development – there is no evidence of a circulation first building in the mid-troposphere and extending downwards (a so-called "top-down" development) (see, e.g., Tory and Montgomery, 2006; Montgomery and Smith 2011).

6.2 | Category 1 Hurricane *Pali*

The track of the low that became Hurricane *Pali* is shown in Figure 10a. Following the demise of TD-9C, the near-equatorial shear zone remained and the MJO remained active with a relatively large amplitude as it progressed from the Western Pacific to the Central Pacific. Within the shear zone, there was a broad counter-clockwise circulation with regions of enhanced positive absolute vorticity and sporadic outbreaks of deep convection. At 0600 UTC on January 5, 2016, a new low had formed within this circulation in the ECMWF analyses with a centre at about 171°W, 3°N. At this time, the position of the low according to the best track data obtained from IBTrACS was analysed to be near 174°W, 2.5°N. It was this low that developed into Hurricane *Pali*.

The evolution of intensity for Hurricane *Pali* and its precursor low is shown in Figure 10b. At 1,000 mb, the maximum wind speed first exceeded 17 m/s at 1800 UTC on January 6 and increased steadily to reach a temporary maximum of 26 m/s at 1200 UTC on January 8. During this period, the vertical shear increased steadily (Figure 10c), reaching a peak of 16 m/s at 0000 UTC on January 9. Possibly as a result of this increase, the low weakened to about 18 m/s, but as the shear weakened also, the low began to intensify again from about 0600 UTC on January 11.

The maximum intensity in the ECMWF analyses is reached at the same time as the best track data at 1800 UTC on January 12, although it is much weaker: 29 m/s compared to 42 m/s. Thereafter, the storm decayed relatively quickly as it tracked back towards the Equator.

6.3 | Vortical and convective environment

Figure 11 shows the 850 mb absolute vorticity, horizontal winds and geopotential height at 850 mb and the vertical *p*-velocity at 500 mb during the development of TD *Pali*. At 1200 UTC on January 4 (Figure 11a), the flow is generally easterly north of the Equator and westerly south of the Equator, the easterlies being punctuated by a cyclonic circulation about the low centred near 176°W, 3°N that is evident by a closed contour in the geopotential height field. At this time, the low is embedded in a large region of positive absolute vorticity that extends southwards to at least 5°S at the longitudes of the low. The low itself coincides with a patch of enhanced absolute vorticity that extends eastsoutheastwards from the low centre to about 1°S. Figure 11b indicates a significant region with areas of vigorous deep convection spanning more than 35° longitude in the region 5°S to 5°N.

By 1200 UTC on January 5, the low has strengthened and the location of the minimum geopotential height has moved eastwards to near 169°W, 3°N (Figure 11c). There is now an elongated band of enhanced positive absolute vorticity north

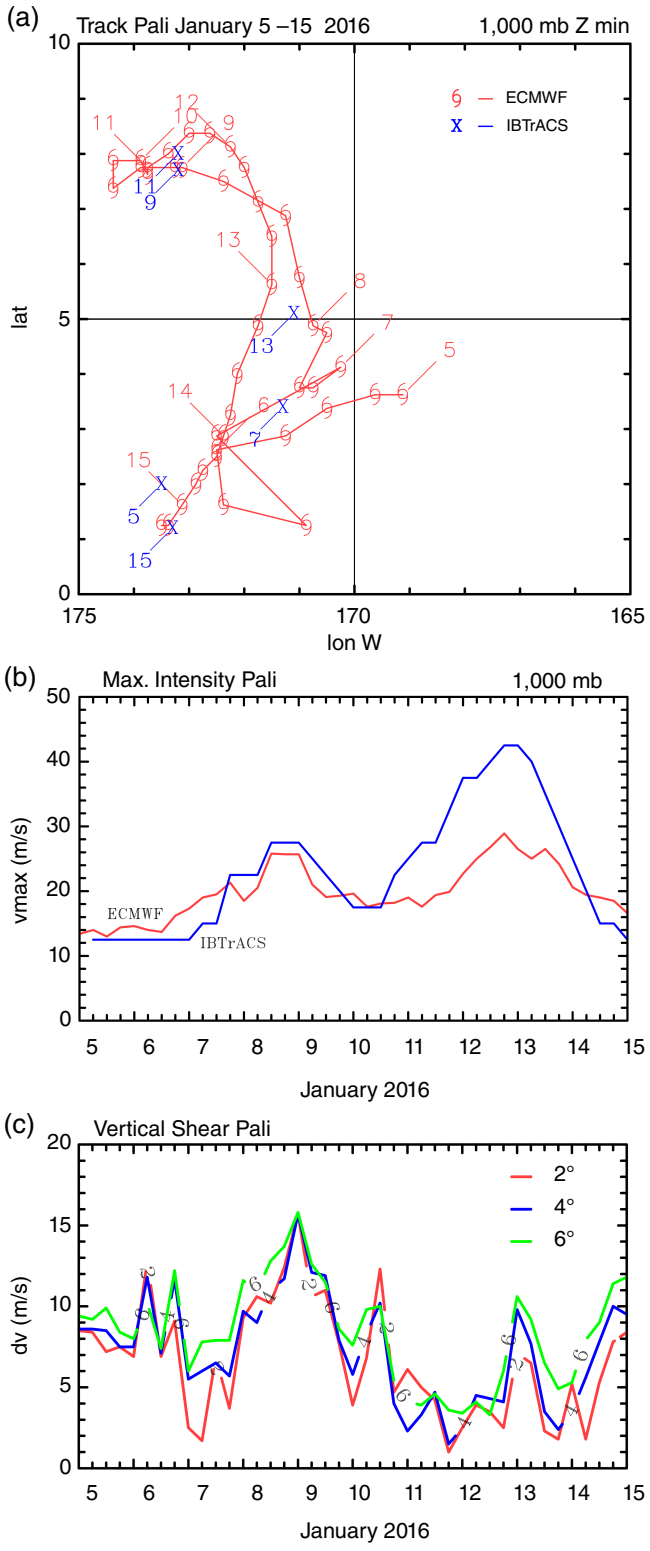

FIGURE 10 (a) Track of TD-1C, which later became Hurricane *Pali*, in the ECMWF analyses (red curve). The blue X symbols indicate the position of *Pali* according to the best track data obtained from IBTrACS. (b) The maximum intensity calculated from the ECMWF analysis data (red curve) with the best track data as given by IBTrACS (blue curve). (c) The column-averaged vertical shear for 2° × 2° (red line), 4° × 4° (blue line) and 6° × 6° (green line) [Colour figure can be viewed at wileyonlinelibrary.com]

of the Equator, south of 6°N, extending more than 35° of longitude. At this time, deep convection is located mostly to the east of the low, but spans a latitude band from about 5°S to 7°N (Figure 11d).

A day later, at 1200 UTC on January 6, the low has strengthened further and its centre has drifted westwards to about 171°W, 2°N (Figure 11e). The central region is now marked by a monopole of enhanced positive absolute vorticity just north of the Equator, but positive absolute vorticity continues to extend beyond 5°S of the Equator. Vigorous deep convection (as defined in sect. 4.3) has become more organized in the region of the low and in a band on its southern side extending westsouthwestwards into the Southern Hemisphere (Figure 11f).

By 1200 UTC on January 7 (Figure 11g,h), the low has deepened further and the vorticity monopole has consolidated in the central region, but the region of positive vorticity south of the Equator has retreated a little and a band of enhanced positive vorticity has formed to the northwest of the centre. The lowest geopotential height is located at about 4°N. Vigorous convection continues to flare close to the vortex centre.

6.3.1 | Bulk properties

Figure 12 shows a series of column-averaged quantities, as in previous cases. During the genesis and early stages of storm intensification, the vertical mass flux in Figure 12a shows regions with positive and negative values between 0000 UTC on January 5 and 0000 UTC on January 6. Thereafter, the mass flux is mostly positive below 600 mb, corresponding with an increase in the circulation (Figure 12b). After 0000 UTC on January 6, the circulation begins to increase at low levels (Figure 12b) and after 0600 UTC on January 7 it increases rapidly through much of the troposphere, the largest circulation values occurring at low levels, typically 900 mb. Again, this is clearly a "bottom-up" development of the vortex. Interestingly, between 1800 UTC on January 7 and 1200 UTC on January 9 the circulation from the surface up to 700 mb in the ECMWF analyses is stronger than during the time period when the storm was classified as Hurricane *Pali*, which was between 1800 UTC on January 11 and 1200 UTC on January 13. Nevertheless, one would not always expect an exact relationship between the circulation around a column and the maximum wind speeds within the column.[4]

As shown in Figure 12c, there is a general warming of the column in the mid- and upper troposphere, with maximum values exceeding 2 K. There is a slight cooling at low levels

[4]The analyses are not perfect as they do not include subjective satellite data which are important for detecting peak wind speeds, and it is unreasonable also to expect a global analysis to accurately identify the peak winds in a small-scale phenomena such as a hurricane.

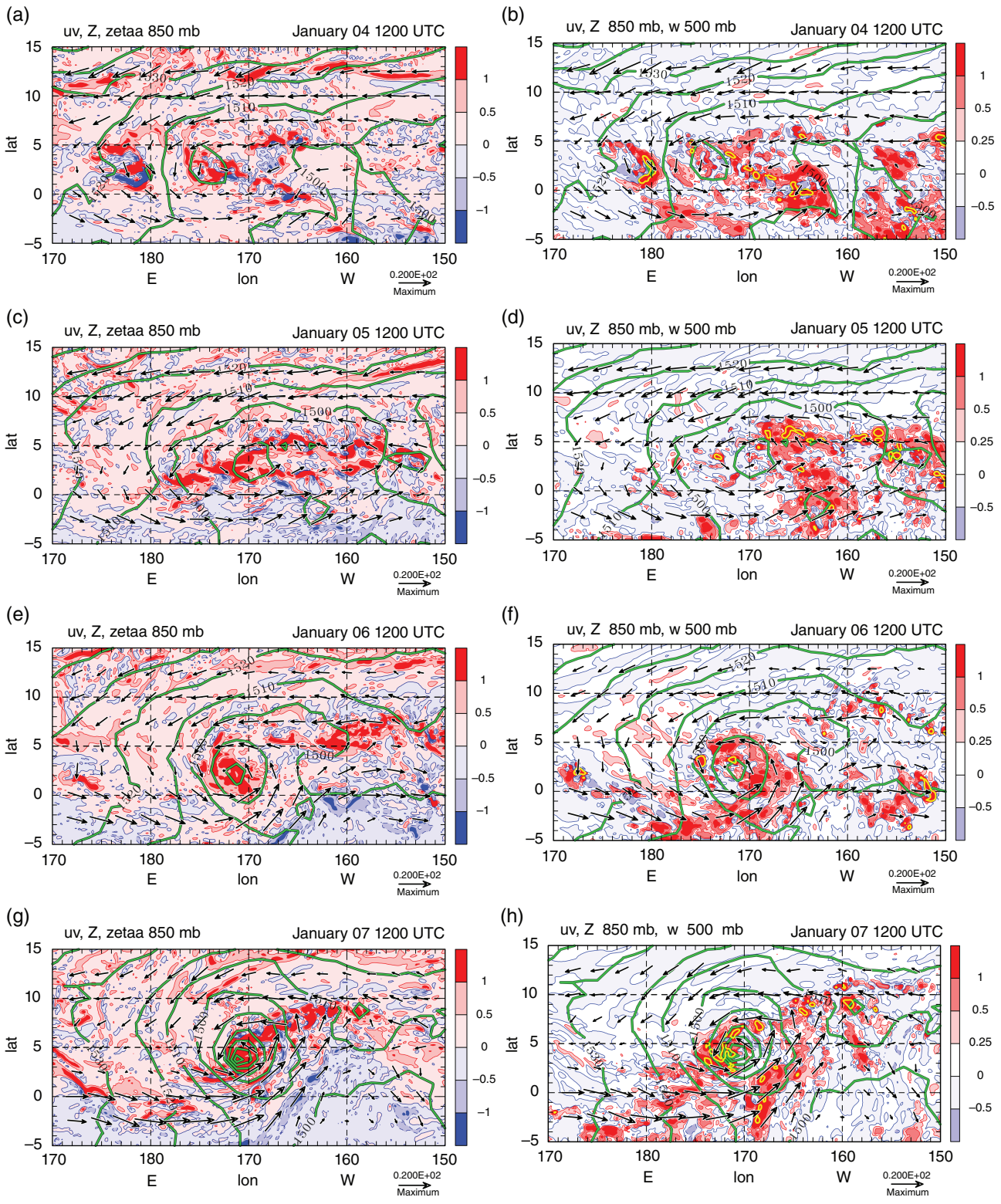

FIGURE 11 Horizontal cross-sections of wind vectors and geopotential height at 850 mb together with absolute vorticity at 850 mb, ζ_a (left panels), and vertical p-velocity at 500 mb, ω (right panels) during the genesis and early evolution of the precursor low of Hurricane *Pali* at the four times shown. The scale for wind vectors is given in m/s at the bottom right. Geopotential height is in geopotential metres (gpm) (solid green contours, interval 10 gpm). In the left panels, the red shading indicates counter-clockwise vorticity (cyclonic in the Northern Hemisphere, anticyclonic in the Southern Hemisphere) and blue shading indicates clockwise vorticity (shading values are multiplied by 1×10^{-4} s^{-1}). In the right panels, positive vertical velocity (negative ω) is shaded red, while negative velocity (positive ω) is shaded light blue (units Pa/s). Red contours: 0.25, 0.5 and 1 Pa/s, respectively. Thick yellow contour: 2 Pa/s

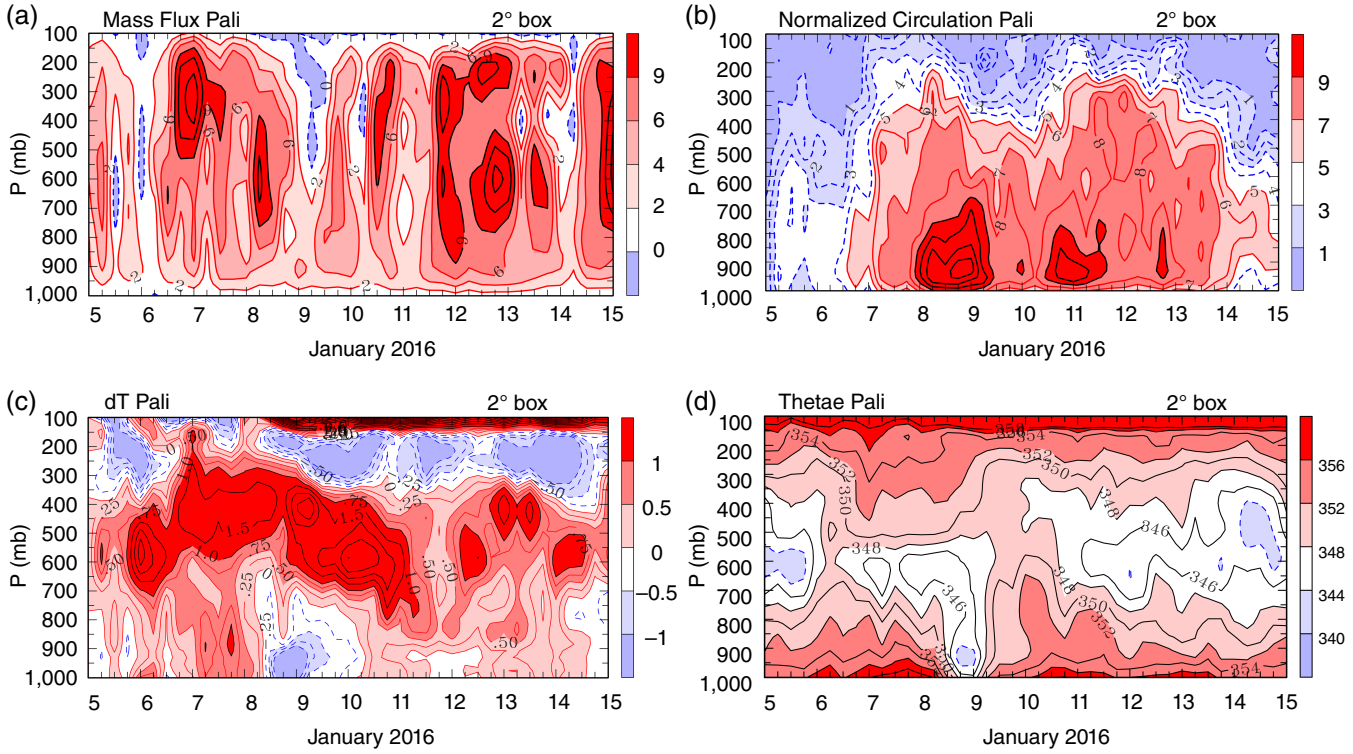

FIGURE 12 Time–height cross-sections of (a) vertical mass flux averaged over a 2° × 2° column centred on the location of the minimum geopotential height at 850 mb for the low that became Hurricane *Pali*, (c) temperature deviation from the start of the series, and (d) and pseudo-equivalent potential temperature. Panel (b) shows the normalized circulation around the 2° × 2° column. The panels have the same descriptions as those in Figure 4 [Colour figure can be viewed at wileyonlinelibrary.com]

that is most prominent on January 8. The time–height series of column-averaged pseudo-equivalent potential temperature θ_e shows a typical tropical pattern for much of the period, with minimum values in the mid-troposphere (Figure 12d). The θ_e minimum is reduced only for brief periods, the most significant being between 0000 UTC on January 9 and 1200 UTC on January 10. There is a short period on January 8 when the values of θ_e fall below 344 K at low levels, a period that coincides with the low-level negative temperature anomalies seen in Figure 12c. These reduced temperatures are presumably associated with convective downdraughts in the inner core region of the storm. Again, the evolution of this system is found to be consistent with those occurring in the Australian monsoon (Smith *et al.*, 2015; Kilroy *et al.*, 2016, 2017b).

6.4 | The demise of TD-9C and the birth of *Pali*

From a forecaster's perspective, conditions for the continued development of TD-9C looked favourable with only moderate vertical wind shear and persistent deep convection occurring near the circulation centre (Figure 9a). To understand why Hurricane *Pali* developed while TD-9C failed to do so within an apparently favourable environment, we examine the possibility that appreciable horizontal shear was a factor. Although regions with enhanced vertical vorticity are favoured locations for vortex formation, this is only true if the vorticity is dominated by pure rotation as opposed to horizontal shear or strain (see, e.g., Dunkerton *et al.*, 2009). Such regions are indicated by positive values of the Okubo–Weiss (OW) parameter defined by

$$OW = \mathrm{Re}\left[\zeta^2 - D^2 - S^2 - 2 \mid D \mid \sqrt{S^2 - \zeta^2}\right], \quad (1)$$

where ζ is the vertical component of relative vorticity, D is the horizontal divergence and S is the total deformation (or strain). These regions are where patches of enhanced vertical vorticity congeal most easily to form a monopole structure. As shown below, the differences in the distributions of OW for TD-9C and the precursor low to Hurricane *Pali* are striking.

Figure 13 shows the distribution of OW at 850 mb for TD-9C at 0000 UTC on December 27 and at 0000 UTC on January 1 (Figure 13a,b), and for the precursor low of Hurricane *Pali* at 0000 UTC on January 6 and 1200 UTC on January 6 (Figure 13c,d). Regions with large horizontal strain and shear values are highlighted by a blue contour. Shown also is a 2° × 2° box centred on the 850 mb geopotential minimum, as well as a contour of 500 mb vertical p-velocity to highlight where deep convection is occurring.

In the early stages of TD-9C at 0000 UTC on December 27, there is a relatively small patch of positive OW within the 2° × 2° box (Figure 13a). This small positive patch is

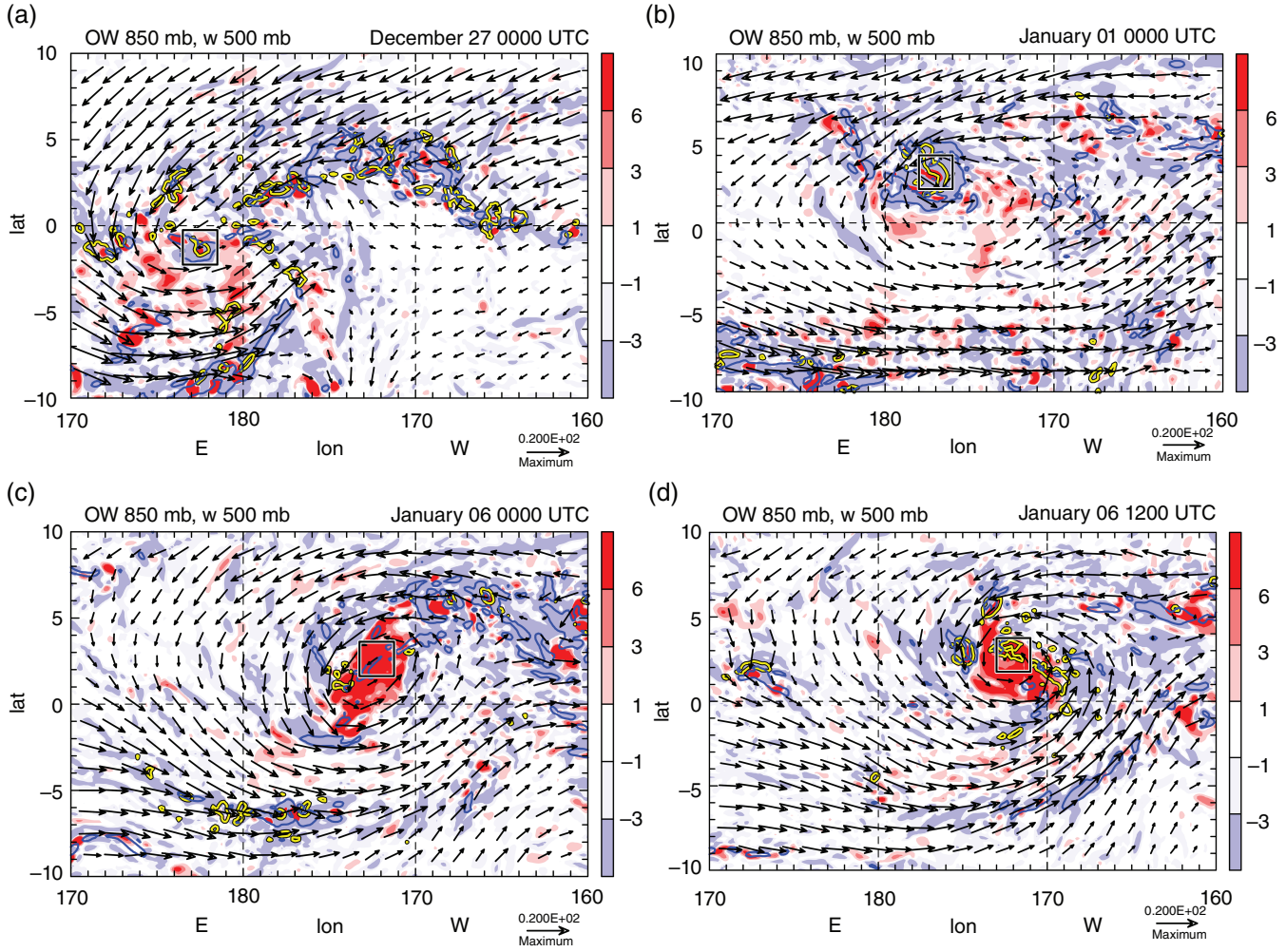

FIGURE 13 Horizontal cross-sections of the Okubo–Weiss parameter at 850 mb for TD-9C (a,b) and the precursor low of Hurricane *Pali* (c,d) at selected times. Shadings are as indicated by the sidebars, multiplied by 10^{-9} s^{-2}. Regions with large strain and shear deformation (1×10^{-9} s^{-2}) are indicated by a blue contour. Shown also are the horizontal wind vectors (black arrows), with the scale given in m/s at the bottom right. The thick yellow contour shows the 500 mb positive vertical velocity (1 Pa/s). Superimposed is a 2° × 2° box (black square) centred on the 850 mb minimum geopotential height

surrounded by regions of negative OW and regions of relatively large horizontal strain and shear deformation. Five days later, just prior to the decay of TD-9C at 0000 UTC on January 1 (Figure 13b), the region of positive OW is still relatively small at the circulation centre; however, the areal extent of the negative OW surrounding the low has increased in size. In particular, there are now large regions of relatively strong strain and shear deformation enveloping the low. Despite persistent convection occurring near the centre of the low, large values of horizontal strain and shear deformation are evidently sufficient to thwart the development of TD-9C.

Five days later at 0000 UTC on January 6 (Figure 13c), the situation has changed significantly. Now the box centred on the low is engulfed and surrounded by large positive values of OW. There are relatively few regions of strong horizontal strain and shear near the centre. At this time there is little deep convective activity within the box, but 12 hr later (Figure 13d) deep convection flares up in and around the box. The box is still engulfed by a large region of positive OW. This region surrounding the circulation centre is favourable for vortex development, where the vorticity is dominated by rotation and where patches of enhanced vertical vorticity congeal most easily to form a monopole structure. In the following days the system begins to intensify as shown by the increase in the ECMWF maximum intensity (Figure 10b).

7 | CONCLUSIONS

We have investigated the formation of tropical cyclones within a few degrees latitude of the Equator, using (for the most part) European Centre for Medium-Range Weather Forecasts (ECMWF) analyses of some prominent events. We demonstrated also the possibility of tropical cyclone formation *at the Equator* using idealized model simulations, starting from a prescribed weak (maximum wind speed

5 m/s) initial vortex in an otherwise quiescent, non-rotating environment.

Three idealized simulations were carried out in which the radius of maximum tangential wind speed was 50, 100 or 150 km. In each case the vortex developed rapidly after a gestation period of between 30 and 60 hr, but it decayed after a few days as the cyclonic angular momentum source provided by the initial vortex was depleted. In these simulations, the larger the initial vortex size, the longer until rapid intensification begins, the larger the maximum intensity attained and the longer the vortex lifetime. The onset time of rapid intensification for all three simulations is almost identical to that in corresponding simulations at 10°N, suggesting that the Coriolis force is not important in the genesis of tropical cyclones. Nevertheless, our results indicate that the Coriolis force *is* important for continued intensification over more than about 2 days.

In the several real events investigated, counter-clockwise rotating vortices formed in a region of counter-clockwise circulation. This circulation encompassed primarily positive absolute vorticity extending 5° or more south of the Equator. In the case of Typhoon *Vamei*, the background circulation was provided by the Borneo vortex, while in the case of Super Typhoon *Dolphin* it appeared to be associated with the unstable roll-up of vorticity in a shear line marking an Intertropical Convergence Zone. In the cases of TD-9C and Hurricane *Pali*, the circulation was associated with a monsoon-like shear line that straddled the Equator. In three of the cases studied (Super Typhoon *Dolphin*, TD-9C and Hurricane *Pali*) there were above-normal sea surface temperatures present in the Central Pacific as a result of strong El Niño conditions, while the MJO was active over the Western Pacific and Central Pacific during the genesis of TD-9C and *Pali*, respectively.

Within the broadscale circulation, patches of absolute vertical vorticity are enhanced as a result of vorticity stretching by deep convection. The patches of enhanced vorticity, which are predominantly counter-clockwise, are organized by the overturning circulation produced by the collective effects of this convection. In the lower troposphere, this overturning circulation fluxes absolute vorticity towards some centre within the convective region. By Stokes' theorem, the tangential circulation about rings of fixed radius around this centre increase and the vortex spins up. At and near the Equator, the absolute vorticity is dominated by the relative vorticity of the background flow. A prominent feature in all cases is that the vortex circulation first developed at low levels in the troposphere, a so-called "bottom-up" development.

Our analyses indicate that the physical processes involved in the genesis and subsequent intensification of the low-latitude storms examined are essentially the same as those found in storms that develop within the Australian monsoon. This result is further evidence that the Earth's background rotation is not a necessary ingredient for tropical cyclogenesis.

There seems to be no intrinsic reason why, at times, regions of negative absolute vorticity should not encroach some distance into the Northern Hemisphere and that clockwise rotating vortices could not form there. We speculate that such a development may occur in conjunction with a westerly wind burst with maximum wind anomalies some way off the Equator (Giese and Harrison, 1991) and in conjunction with a positive phase of the MJO where there is enhanced convective activity. However, we know of no such occurrences that have been documented.

ACKNOWLEDGEMENTS

We thank two anonymous reviewers for their perceptive comments on the original manuscript. We thank Michael Montgomery also for his early feedback on the study and Dr. Nils Wedi for providing information about the ECMWF analysis and forecast system. The ECMWF analyses were kindly made available by the German Weather Service (Deutscher Wetterdienst). Thanks also to the following individuals who all promptly provided us with the best track data of Hurricane *Pali*: Dr. John Knaff, NESDIS/STAR, CIRA/Colorado State University; Dr. Patrick Duran, Earth System Science Center, University of Alabama in Huntsville; Dr. Howard Diamond, NOAA; and Dr. James P. Kossin, NOAA's National Centers for Environmental Information (NCEI) Center for Weather and Climate, Madison, WI. Gerard Kilroy was supported by the Deutsche Forschungsgemeinschaft (German Research Council) under grant KO 2248/2-1.

REFERENCES

Anthes, R.S. (1982) *Tropical Cyclones: Their Evolution, Structure and Effects*. Boston, MA: American Meteorological Society.

Bryan, G.H. and Fritsch, J.M. (2002) A benchmark simulation for moist nonhydrostatic numerical models. *Monthly Weather Review*, 130, 2917–2928.

Chang, C.P. and Wong, T.S. (2008) Rare typhoon development near the equator. In: Liou, K.N., Chou, M.D. and Hsu, H.H. (Eds.) *Recent Progress in Atmospheric Sciences: Applications to the Asia-Pacific Region*. Singapore: World Scientific, pp. 172–181.

Chang, C.P., Liu, C.H. and Kuo, H.C. (2003) Typhoon Vamei: an equatorial tropical cyclone formation. *Geophysical Research Letters*, 30, 1150.

Dunkerton, T.J., Montgomery, M.T. and Wang, Z. (2009) Tropical cyclogenesis in a tropical wave critical layer: easterly waves. *Atmospheric Chemistry and Physics*, 9, 5587–5646.

Emanuel, K.A. (2005) *Divine Wind: The History and Science of Hurricanes*. New York: Oxford University Press.

Ferreira, R.N. and Schubert, W.H. (1997) Barotropic aspects of ITCZ breakdown. *Journal of the Atmospheric Sciences*, 54, 261–285.

Giese, B.S. and Harrison, D.E. (1991) Eastern equatorial Pacific response to three composite westerly wind types. *Journal of Geophysical Research*, 96, 3239–3248.

Gill, A.E. (1982) *Atmosphere–Ocean Dynamics*. London: Academic Press.

Houze, R.A. (1993) *Cloud Dynamics*. San Diego, CA: Academic Press.

Hendricks, E.A., Montgomery, M.T. and Davis, C.A. (2004) The role of "vortical" hot towers in the formation of Tropical Cyclone Diana (1984). *Journal of the Atmospheric Sciences*, 61, 1209–1232.

Hobgood, J. (2018) The myth that tropical cyclones can't form near the Equator *33rd American Meteorological Society Conference on Hurricanes and Tropical Meteorology, April 2018, Ponte Vedra, FL*. Boston, MA: American Meteorological Society.

Houston, S. and Birchard, T. (2016) *NOAA Central Pacific Hurricane Center Tropical Cyclone report: Tropical Depression Nine-C* p. CP092015. Available at: http://www.prh.noaa.gov/cphc/summaries/ [Accessed July 2018].

Juneng, L., Tangang, F.T., Reason, C.J.C., Moten, S. and Hassan, W.A.W. (2007) Simulation of Tropical Cyclone Vamei (2001) using the PSU/NCAR MM5 Model. *Meteorology and Atmospheric Physics*, 97, 273–290.

Kilroy, G. and Smith, R.K. (2016) A numerical study of deep convection in tropical cyclones. *Quarterly Journal of the Royal Meteorological Society*, 142, 3138–3151.

Kilroy, G. and Smith, R.K. (2017) The effects of initial vortex size on tropical cyclogenesis and intensification. *Quarterly Journal of the Royal Meteorological Society*, 143, 2832–2845.

Kilroy, G., Smith, R.K., Montgomery, M.T., Lynch, B. and Earl-Spurr, C. (2016) A case study of monsoon low that formed over the sea and intensified over land as seen in the ECMWF analyses. *Quarterly Journal of the Royal Meteorological Society*, 142, 2244–2255.

Kilroy, G., Smith, R.K. and Montgomery, M.T. (2017a) A unified view of tropical cyclogenesis and intensification. *Quarterly Journal of the Royal Meteorological Society*, 143, 450–462.

Kilroy, G., Smith, R.K. and Montgomery, M.T. (2017b) Tropical low formation and intensification over land as seen in ECMWF analyses. *Quarterly Journal of the Royal Meteorological Society*, 143, 772–784.

Knapp, K.R., Kruk, M.C., Levinson, D.H., Diamond, H.J. and Neumann, C.J. (2010) The International Best Track Archive for Climate Stewardship (IBTrACS): unifying tropical cyclone best track data. *Bulletin of the American Meteorological Society*, 91, 363–376.

Koseki, S., Koh, T.-Y. and Teo, C.-K. (2014) Borneo vortex mesoscale convective rainfall. *Atmospheric Chemistry and Physics*, 14, 4539–4562.

Montgomery, M.T. and Smith, R.K. (2011) Tropical-cyclone formation: theory and idealized modelling. *Proceedings of the Seventh WMO International Workshop on Tropical Cyclones (IWTC-VII), November 2010, La Réunion*. Geneva: World Meteorological Organization. http://www.wmo.int/pages/prog/arep/wwrp/tmr/otherfileformats/documents/2_1.pdf.

Montgomery, M.T. and Smith, R.K. (2014) Paradigms for tropical-cyclone intensification. *Australian Meteorological and Oceanographic Journal*, 64, 37–66.

Montgomery, M.T. and Smith, R.K. (2017) Recent developments in the fluid dynamics of tropical cyclones. *Annual Review of Fluid Mechanics*, 49, 541–574.

Montgomery, M.T., Nicholls, M.E., Cram, T.A. and Saunders, A.B. (2006) A vortical hot tower route to tropical cyclogenesis. *Journal of the Atmospheric Sciences*, 63, 355–386.

Nguyen, S.V., Smith, R.K. and Montgomery, M.T. (2008) Tropical-cyclone intensification and predictability in three dimensions. *Quarterly Journal of the Royal Meteorological Society*, 134, 563–582.

Ooyama, K.V. (1969) Numerical simulation of the life cycle of tropical cyclones. *Journal of the Atmospheric Sciences*, 26, 3–40.

Phillips, N.A. (1966) The equations of motion for a shallow rotating atmophere and the "traditional approximation". *Journal of the Atmospheric Sciences*, 23, 626–628.

Pielke, R.A., Jr. and Pielke, R.A., Sr. (1997) *Hurricanes: Their Nature and Impacts on Society*. New York: John Wiley & Sons.

Smith, R.K. and Montgomery, M.T. (2016) The efficiency of diabatic heating and tropical cyclone intensification. *Quarterly Journal of the Royal Meteorological Society*, 142, 2081–2086.

Smith, R.K., Montgomery, M.T., Kilroy, G., Tang, S. and Müller, S.K. (2015) Tropical low formation during the Australian monsoon: the events of January 2013. *Australian Meteorological and Oceanographic Journal*, 65, 318–341.

Smith, R.K., Zhang, J.A. and Montgomery, M.T. (2017) The dynamics of intensification in an HWRF simulation of Hurricane Earl (2010). *Quarterly Journal of the Royal Meteorological Society*, 143, 293–308.

Tory, K. and Montgomery, M.T. (2006) Internal influences on tropical cyclone formation *The Sixth WMO International Workshop on Tropical Cyclones (IWTC-VI), November 2006, Costa Rica, San José*. Geneva: World Meteorological Organization. http://severe.worldweather.wmo.int/iwtc/document/BW_IWTC-VI_pre-workshop_v12.pdf.

Wallace, J.M. and Hobbs, P.V. (2006) *Atmospheric Science: An Introductory Survey*, 2nd edition. Amsterdam: Academic Press/Elsevier.

Wissmeier, U. and Smith, R.K. (2011) Tropical-cyclone convection: the effects of ambient vertical vorticity. *Quarterly Journal of the Royal Meteorological Society*, 137, 845–857.

How to cite this article: Steenkamp SC, Kilroy G, Smith RK. Tropical cyclogenesis at and near the Equator. *Q J R Meteorol Soc*. 2019;145:1846–1864. https://doi.org/10.1002/qj.3529